THE JOURNAL OF BIOLOGICAL CHEMISTRY VOL. 286, NO. 19, pp. 16940–16952, May 13, 2011

Involvement of Dominant-negative Spliced Variants of the Intermediate Conductance Ca^{2+}-activated K^+ Channel, $K_{Ca}3.1$, in Immune Function of Lymphoid Cells*[S]

Received for publication, September 13, 2010, and in revised form, January 24, 2011 Published, JBC Papers in Press, February 23, 2011, DOI 10.1074/jbc.M110.184192

Susumu Ohya, Satomi Niwa, Ayano Yanagi, Yuka Fukuyo, Hisao Yamamura, and Yuji Imaizumi[1]

From the Department of Molecular and Cellular Pharmacology, Graduate School of Pharmaceutical Sciences, Nagoya City University, Nagoya 467-8603, Japan

The intermediate conductance Ca^{2+}-activated K^+ channel (IK_{Ca} channel) encoded by $K_{Ca}3.1$ is responsible for the control of proliferation and differentiation in various types of cells. We identified novel spliced variants of $K_{Ca}3.1$ (human (h) $K_{Ca}3.1b$) from the human thymus, which were lacking the N-terminal domains of the original $hK_{Ca}3.1a$ as a result of alternative splicing events. $hK_{Ca}3.1b$ was significantly expressed in human lymphoid tissues. Western blot analysis showed that $hK_{Ca}3.1a$ proteins were mainly expressed in the plasma membrane fraction, whereas $hK_{Ca}3.1b$ was in the cytoplasmic fraction. We also identified a similar N terminus lacking $K_{Ca}3.1$ variants from mice and rat lymphoid tissues ($mK_{Ca}3.1b$ and $rK_{Ca}3.1b$). In the HEK293 heterologous expression system, the cellular distribution of cyan fluorescent protein-tagged $hK_{Ca}3.1a$ and/or YFP-tagged $hK_{Ca}3.1b$ isoforms showed that $hK_{Ca}3.1b$ suppressed the localization of $hK_{Ca}3.1a$ to the plasma membrane. In the *Xenopus* oocyte translation system, co-expression of $hK_{Ca}3.1b$ with $hK_{Ca}3.1a$ suppressed IK_{Ca} channel activity of $hK_{Ca}3.1a$ in a dominant-negative manner. In addition, this study indicated that up-regulation of $mK_{Ca}3.1b$ in mouse thymocytes differentiated CD4(+)CD8(+) phenotype thymocytes into CD4(−)CD8(−) ones and suppressed concanavalin-A-stimulated thymocyte growth by down-regulation of mIL-2 transcripts. Anti-proliferative effects and down-regulation of mIL-2 transcripts were also observed in $mK_{Ca}3.1b$-overexpressing mouse thymocytes. These suggest that the N-terminal domain of $K_{Ca}3.1$ is critical for channel trafficking to the plasma membrane and that the fine-tuning of IK_{Ca} channel activity modulated through alternative splicing events may be related to the control in physiological and pathophysiological conditions in T-lymphocytes.

The Ca^{2+}-activated K^+ (K_{Ca}) channel is a family of the K^+ channel superfamily that can directly communicate with Ca^{2+} signal pathways and is responsible for various cellular processes by controlling membrane potential. In nonexcitable cells, hyperpolarization of the membrane potential, which is induced by activation of the K_{Ca} channel, increases the driving force for Ca^{2+} entry. Activation of the K_{Ca} channel is therefore strongly associated with sustained Ca^{2+} influx and the Ca^{2+}-dependent signaling pathway (1, 2). The intermediate conductance K_{Ca} channel (IK_{Ca})[2] is present in a variety of non-neuronal peripheral tissues, *e.g.* spleen, thymus, peripheral blood leukocytes, T-lymphocytes, and undifferentiated vascular smooth muscles, and it participates in the control of cell proliferation and migration (3, 4). Physiological roles of $K_{Ca}3.1$ in T-lymphocytes are as follows: 1) maintenance of the intracellular Ca^{2+} levels required for mitogen activation by membrane potential hyperpolarization (5, 6), and 2) the control of apoptotic cell volume decrease, the initiation step in Ca^{2+}-induced apoptosis (7). Recent studies have shown that IK_{Ca} channels are possible molecular targets for pharmacological intervention in various diseases, *e.g.* autoimmune diseases, restenosis, urinary incontinence, and cystic fibrosis (8–11).

Four subtypes of small/intermediate conductance Ca^{2+}-activated K^+ channels ($K_{Ca}2.1$, $K_{Ca}2.3$, and $K_{Ca}3.1$) have been identified by molecular cloning studies and are activated via a mechanism involving Ca^{2+} binding to the EF hands of calmodulin (4, 12, 13). $K_{Ca}2.x$ and $K_{Ca}3.1$ can make heteromeric complexes of four pore-forming α subunits with different pharmacological profiles and cell surface expression from homotetramers (14, 15). Additionally, alternative splicing is a common mechanism for generating K^+ channel diversity (16). Of interest, two alternatively spliced variants of $K_{Ca}2.3$, $K_{Ca}2.3$–1B and $K_{Ca}2.3$–1C, which have a different first exon from the original $K_{Ca}2.3$ and thereby lack transmembrane segment 1 (S1), have caused dominant-negative suppression of $K_{Ca}2.x$ and $K_{Ca}3.1$ by trapping these channel proteins intracellularly (14, 15, 17). For example, $K_{Ca}2.3$–1B, which is implicated in schizophrenia (15, 18), suppresses $K_{Ca}2.1$ channel activity in human Jurkat T cells, and $K_{Ca}2.3$–1C suppresses $K_{Ca}2.x$ and $K_{Ca}3.1$ channel activities

* This work was supported by a Grant-in-aid for Scientific Research (C) 21590098 from the Ministry of Education, Culture, Sports, Science and Technology, Japan (to S. O.), the Salt Science Research Foundation Grant 10C6 (to S. O.), Takeda Science Foundation (to S. O.), a grant-in-aid for scientific research (B) from the Ministry of Education, Culture, Sports, Science and Technology (to Y. I.), and Grant-in-aid for Scientific Research on Priority Areas 20056027 from the Ministry of Education, Culture, Sports, Science and Technology (to Y. I.).

[S] The on-line version of this article (available at http://www.jbc.org) contains supplemental Figs. S1–S8 and Table S1.

The nucleotide sequence(s) reported in this paper has been submitted to the DDBJ/GenBank™/EBI Data Bank with accession number(s) AB128983, AB128984, AB128985, AB128930, AB292802, and AB292803.

[1] To whom correspondence should be addressed: Molecular and Cellular Pharmacology, Graduate School of Pharmaceutical Sciences, Nagoya City University, 3-1 Tanabedori, Mizuhoku, Nagoya 467-8603, Japan. Tel./Fax: 81-52-836-3431; E-mail: yimaizum@phar.nagoya-cu.ac.jp.

[2] The abbreviations used are: IK_{Ca}, intermediate conductance K_{Ca} channel; MTT, 3-(4,5-dimethylthiazol-2-yl)-2,5-diphenyltetrazolium bromide; CFP, cyan fluorescent protein; h, human; m, murine; r, rat; DIS, dominant-inhibitory segment; ChTX, charybdotoxin; DN, double-negative; DP, double-positive; Con-A, concanavalin-A; DC-EBIO, 5,6-dichloro-1-ethyl-1,3-dihydro-2*H*-benzimidazol-2-one.

almost completely and $K_{Ca}3.1$ channel activity partially. Kolski-Andreaco *et al.* (17) found that the dominant-inhibitory segment (DIS) in the C terminus plays an essential role in $K_{Ca}2/3$ subunit interaction and reduces functional $K_{Ca}2/3$ channel expression on the cell surface. Several reports have shown that the cell surface trafficking of $K_{Ca}3.1$ is modulated by calmodulin and C-terminal leucine zipper (19, 20); however, the dominant-negative $K_{Ca}3.1$ isoforms have not been identified yet.

In this study, we identified the alternatively spliced variants of $K_{Ca}3.1$ ($K_{Ca}3.1$-ΔN) in lymphoid tissues of humans, mice, and rats and examined their tissue distribution using real time PCR and Western blot analyses. Also, the dominant-negative regulation of the original $K_{Ca}3.1a$ by $K_{Ca}3.1$-ΔN was determined by fluorescence imaging and electrophysiological techniques. Furthermore, to clarify the physiological significance of $K_{Ca}3.1$-ΔN in immune function, we examined the functional impacts of increased $K_{Ca}3.1$-ΔN on mouse thymocyte proliferation and CD4/CD8 thymocyte subsets using cell proliferation assay and flow cytometry analysis, respectively. The role of $K_{Ca}3.1b$ in mouse thymocytes was also examined by generating $mK_{Ca}3.1b$-overexpressing thymocytes.

EXPERIMENTAL PROCEDURES

RNA Extraction, RT-PCR, and Real Time PCR—Total RNA extraction and RT-PCR from mice and rats were performed as reported previously (21). All experiments were carried out in accordance with the guiding principles for the care and use of laboratory animals (Science and International Affairs Bureau of the Japanese Ministry of Education, Science, Sports and Culture) and also with the approval of the ethics committee at Nagoya City University. Human RNA was purchased from Invitrogen. The resulting cDNA product was amplified with gene-specific primers (21), and primers are designated using Primer Express™ software (version 1.5; Applied Biosystems, Foster City, CA) (supplemental Table S1). The amplification profile was follows: a 15-s denaturation step at 96 °C and a 1–2-min primer extension step at 60 °C. The amplified products were separated on 1.0–2.5% agarose gels and visualized by ethidium bromide staining. Obtained full-length $K_{Ca}3.1$ clones were ligated into pBluescript SK(+) (Stratagene, La Jolla, CA) and pECFP-C1/pEYFP-C1 (BD Biosciences, Palo Alto, CA). To confirm the nucleotide sequences, amplified PCR products and plasmid constructs were sequenced with an ABI PRIZM 3100 genetic analyzer (Applied Biosystems).

Real time quantitative PCR was performed using SYBR Green chemistry on an ABI 7000 sequence detector system (Applied Biosystems) as reported previously (21). Regression analysis of the mean values of four multiplex RT-PCRs for $\log_{10}$ diluted cDNA was used to generate standard curves. Unknown quantities relative to the standard curve for a particular set of primers were calculated, yielding transcriptional quantification of the gene products for $K_{Ca}3.1$ spliced variants relative to the endogenous standard, glyceraldehyde-3-phosphate dehydrogenase (GAPDH).

Western Blot, Immunoprecipitation, and Immunocytochemistry—Protein fractions of the plasma membrane and cytoplasmic region were prepared from mouse and rat tissues as reported previously (21), and those from human tissues were purchased from the BioChain Institute (Hayward, CA). Protein fractions were solubilized with 2× sample buffer with 1% SDS and subjected to SDS-PAGE (10%). The blots were incubated with anti-$K_{Ca}3.1$ antibody specific to the C-terminal region (anti-$K_{Ca}3.1$-C; Alomone Labs, Jerusalem, Israel) and then incubated with anti-rabbit horseradish peroxidase-conjugated IgG (Chemicon International, Inc., Temecula, CA). An enhanced chemiluminescence detection system (Amersham Biosciences) was used for the detection of the bound antibody. Resulting images were analyzed by a LAS-1000 device (Fujifilm, Tokyo, Japan).

For immunoprecipitation, cells and tissue homogenates from the mouse thymus were incubated with anti-$K_{Ca}3.1$ antibody specific to the N-terminal region (anti-$K_{Ca}3.1$-N, ab65985; Abcam, Cambridge, MA) overnight at 4 °C, and immunoprecipitation was performed using the Seize Classic mammalian immunoprecipitation kit according to the experimental manual supplied by Pierce. After the obtained fractions were subjected to SDS-PAGE, the blots were incubated with anti-$K_{Ca}3.1$-C (Alomone Labs) antibody, and the images were detected as described above. Immunocytochemical staining of $K_{Ca}3.1$ in mouse thymocytes was performed as shown in our previous report (21), and Alexa Fluor® 488 goat anti-rabbit IgG (Invitrogen) was used as a secondary antibody.

Subcellular Localization of $K_{Ca}3.1$ Spliced Variants—To visualize the intracellular distribution of human and mouse $K_{Ca}3.1$ spliced variants by laser scanning confocal microscopy (LSM 510; Carl Zeiss, Oberkochen, Germany), the full-length of $hK_{Ca}3.1a$–d and $mK_{Ca}3.1a$ and -b clones was subcloned into pECFP-C1 and pEYFP-C1, and each plasmid construct was referred to as pECFP-$hK_{Ca}3.1a$, pEYFP-$hK_{Ca}3.1b$, pEYFP-$hK_{Ca}3.1c$, pEYFP-$hK_{Ca}3.1d$, pECFP-$mK_{Ca}3.1a$, and pEYFP-$mK_{Ca}3.1b$. HEK293 cell line (Health Science Research Resources Bank (HSRRB), Tokyo, Japan) was maintained as reported previously (21). Cells were transiently transfected with plasmid constructs using Lipofectamine 2000 reagent (Invitrogen). Cells were used in the experiments 48–72 h after transfection. Control cells were transfected with plasmid vector alone. Spectral line profiles of the fluorescence and quantification of fluorescent signals were performed using Image-Pro Plus software (version 5.1; Silver Spring, MD) and Image J software (version 1.42, National Institutes of Health). The fluorescence intensity in and below the plasma membrane within 1.0 μm was calculated. Confocal parameters were set such that pixel saturation was less than 10% and that signal intensities were in the linear range of photomultiplier sensitivity.

RNA Injection to Oocytes and Electrophysiology—Adult female *Xenopus laevis* frogs were purchased from Hamamatsu Seibutsu Kyozai (Shizuoka, Japan) and maintained in the laboratory until used. The specific cRNA for hSK4a–d was synthesized *in vitro* from the linearized plasmids using the mMESSAGE mMACHINE™ *in vitro* transcription kit (Ambion, Austin, TX). Defolliculated stage V and VI *X. laevis* oocytes were harvested, and 50 nl of cRNA per oocyte was injected at a concentration of 0.5–1.0 μg/μl using a microinjector. Oocytes were incubated at 20 °C in standard ND96 solution (in mM: 96 NaCl, 2 KCl, 1.8 $CaCl_2$, 1 $MgCl_2$, and 5 HEPES, pH

7.4, adjusted with NaOH) supplemented with antibiotics to permit channel expression. One or 2 days after the injection of cRNA, oocytes were voltage-clamped using two microelectrodes (22). Membrane currents were recorded using an amplifier (CEZ-1250; Nihon Koden, Tokyo, Japan) and a pen recorder (FBR-252A; DKK-TOA, Tokyo, Japan). All experiments were performed at room temperature (23 ± 1 °C). Ionomycin, DC-EBIO, and charybdotoxin were purchased from Sigma, Tocris Bioscience (Ellisville, MO), and Peptide Institute Inc. (Osaka, Japan), respectively.

Preparation of Concanavalin-A-stimulated Mouse Thymocytes and Excess Expression of EYFP-fused $mK_{Ca}3.1b$ in Primary Cultured Thymocytes—Mouse thymocytes were prepared by pressing the thymus with frosted slide glasses in the medium containing RPMI 1640 (Invitrogen) supplemented with 10% heat-inactivated fetal calf serum (Invitrogen) and antibiotics (penicillin and streptomycin) in the presence and absence of concanavalin-A (Con-A, 5 μg/ml) (Con-A(+) and Con-A(−), respectively). After 60 min, Con-A(−) thymocytes were cultivated with Con-A-supplemented medium for 0–2 days. Primary cultured Con-A(+) thymocytes were transiently transfected with pEYFP-C1 (control vector alone) or pEYFP-$mK_{Ca}3.1b$ using Lipofectamine LTX with Plus reagent (Invitrogen). Cells were used in the experiments 2 days after transfection. Determination of maximal efficacy was performed according to the manufacturer's instructions.

Measurement of Mouse Thymocyte Viability by MTT Assay—MTT (Sigma) cell proliferation assay was performed to assess the viability of mouse thymocytes. Briefly, 4×10^5 cells/ml were cultured in duplicate in 96-well plates for 0–2 days. After addition of MTT reagent into each well, lysing solution was added, and the absorbance was measured in a multiple well plate reader, Multiscan JX (Thermo Electron Corp., Waltham, MA) at a test wavelength of 540 nm and a reference wavelength of 630 nm. TRAM-34 was purchased from Santa Cruz Biotechnology (Santa Cruz, CA).

Flow Cytometric Analysis—Cell surface markers were analyzed with a FACScan flow cytometer (BD LSR, BD Biosciences) acquiring at least 10,000 events. Data were analyzed using CellQuest software (BD Biosciences). The lymphocyte gate was established by analysis of forward angle *versus* right angle light scatter. The percentage of positive-staining cells was determined by comparing test histograms with those obtained using fluorescein isothiocyanate (FITC)-labeled CD4 and phycoerythrin-labeled CD8 antibodies (BD Biosciences).

Apoptosis Measurement by Annexin V Staining—Apoptotic cells were analyzed with annexin V-EGFP or -phycoerythrin apoptosis detection kit (Medical and Biological Laboratories (MBL), Nagoya, Japan) by confocal laser microscopy (A1R, Nikon, Tokyo, Japan). Annexin V staining was performed according to the manufacturer's instructions.

Statistical Analysis—Statistical significance between and among multiple groups was evaluated using Student's *t* test, Welch's *t* test, or Tukey's test after *F* test or analysis of variance. Data are presented as the means ± S.E.

RESULTS

Molecular Cloning of Alternatively Spliced Variants of $K_{Ca}3.1$ in Human, Murine, and Rat Thymus—We first examined $K_{Ca}3.1$ protein expression in the mouse thymus and spleen by Western blotting using anti-$K_{Ca}3.1$C antibody. Unexpectedly, band signal with a smaller molecular weight (around 30 kDa) than predicted from mouse $K_{Ca}3.1$ (around 50 kDa) was detected, and disappeared by preincubation of primary anti-$K_{Ca}3.1$C antibody with excess antigen (supplemental Fig. S1). We then designed specific PCR primers to isolate full-length $K_{Ca}3.1$ from human thymus (see supplemental Table S1), and two different fragments were detected (data not shown). As in the results from DNA sequencing, we identified novel $K_{Ca}3.1$ spliced variants, named $hK_{Ca}3.1b$ (Fig. 1*A*, amino acid sequences, and supplemental Fig. S2*A*, nucleotide sequences). In addition, from much less abundant PCR fragments, we also identified two additional $K_{Ca}3.1$ spliced variants, $hK_{Ca}3.1c$ and $hK_{Ca}3.1d$ (Fig. 1*A* and supplemental Fig. S2*A*). Ghanshani *et al.* (25) have shown that human $K_{Ca}3.1$ is composed of nine exons on chromosome 19q13.2. On the basis of genomic sequence information of human $K_{Ca}3.1$ (GenBank™ accession number, NT_011109), $hK_{Ca}3.1b$ lacked partial sequences of exon 2 and/or exon 3 compared with original $K_{Ca}3.1$ ($hK_{Ca}3.1a$) (supplemental Fig. S2*D*), resulting in the truncation of N-terminal transmembrane segments from S1 to S3. We also isolated rodent $K_{Ca}3.1$ spliced variants, named $mK_{Ca}3.1b$ (Fig. 1*B* and supplemental Fig. S2*B*) and $rK_{Ca}3.1b$ (Fig. 1*C* and supplemental Fig. S2*C*) from mouse and rat thymus. $mK_{Ca}3.1b$ lacked exon 3 but gained a novel exon 4, exon 4a, compared with the original $mK_{Ca}3.1$, $mK_{Ca}3.1a$, resulting in the truncation of N-terminal sequences (S1–S5) (supplemental Fig. S2*Db*). $rK_{Ca}3.1b$ lacked exon 2 and partial sequences of exon 1 and exon 3, also resulting in the truncation of N-terminal sequences (S1–S4). We also found an additional $rK_{Ca}3.1$ variant, $rK_{Ca}3.1c$, with different C-terminal sequences from original $rK_{Ca}3.1a$, lacking exon 7 and exon 8; however, $rK_{Ca}3.1c$ was a much less abundant isoform than $rK_{Ca}3.1a$ as a result of competitive PCR assay (data not shown).

Transcriptional Expression of $K_{Ca}3.1$ Spliced Variants in Human, Mouse, and Rat Tissues—Human $K_{Ca}3.1$ transcripts are expressed in a variety of peripheral tissues, *e.g.* thymus, spleen, placenta, prostate, lung, stomach, urinary bladder, and colon (12, 13). To identify the relative expression levels of $K_{Ca}3.1$ spliced variants in human, mouse, and rat tissues, we performed real time PCR analyses using specific primers for the following: (i) $hK_{Ca}3.1a/b$; (ii) $hK_{Ca}3.1a$; (iii) $mK_{Ca}3.1a/b$; (iv) $mK_{Ca}3.1a$; (v) $mK_{Ca}3.1b$; (vi) $rK_{Ca}3.1a/b$; and (vii) $rK_{Ca}3.1a$ (see supplemental Table S1). In human tissues, expressions of $K_{Ca}3.1a$ and $K_{Ca}3.1b$ isoforms ($K_{Ca}3.1a/b$) relative to an internal standard, GAPDH, were 0.045, 0.014, 0.049, 0.053, 0.027, and 0.011 in the thymus, spleen, lymph node, placenta, colon, and urinary bladder (bladder), whereas $hK_{Ca}3.1a$ expressions were 0.035, 0.008, 0.006, 0.017, 0.010, and 0.008 (mean values in triplicate) (Fig. 2*A*). Taken together, $hK_{Ca}3.1b$ transcripts were expressed in human tissues examined at various levels, and its predominant expression was observed in the lymph nodes and placenta. Additionally, in mouse tissues, $mK_{Ca}3.1a$ expressions

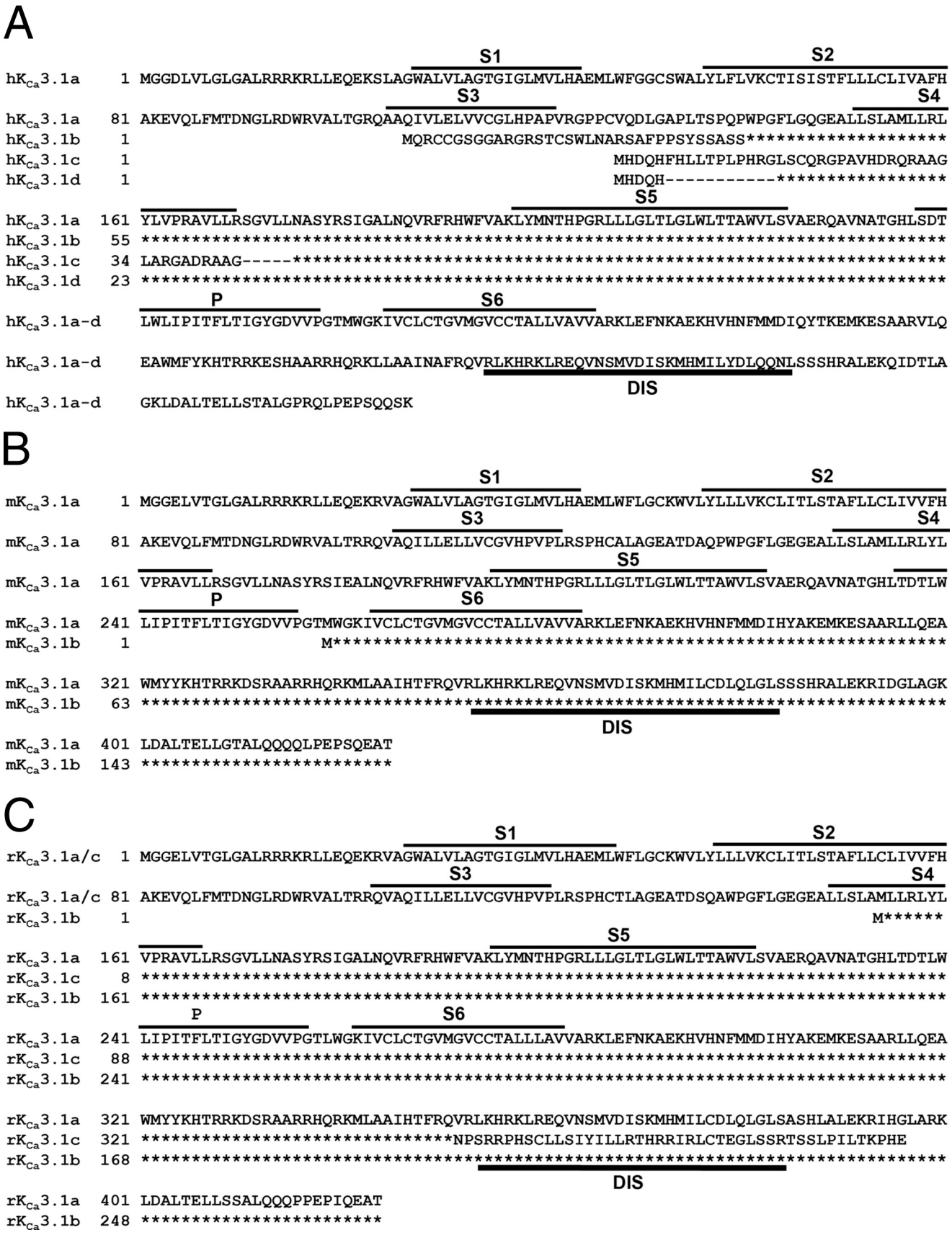

FIGURE 1. **Alternatively spliced variants of $K_{Ca}3.1$.** The alignment of the amino acid sequences of human (*A*), mouse (*B*), and rat (*C*) $K_{Ca}3.1$ ($hK_{Ca}3.1$, $mK_{Ca}3.1$, and $rK_{Ca}3.1$) spliced variants. Residues identical to the original $K_{Ca}3.1$, $K_{Ca}3.1a$, are shown as *asterisks*, and *dashes* indicate gaps introduced into the sequence to improve alignment. *S1–S6* and *P* indicate the transmembrane segment 1–6 and pore-forming domain, respectively.

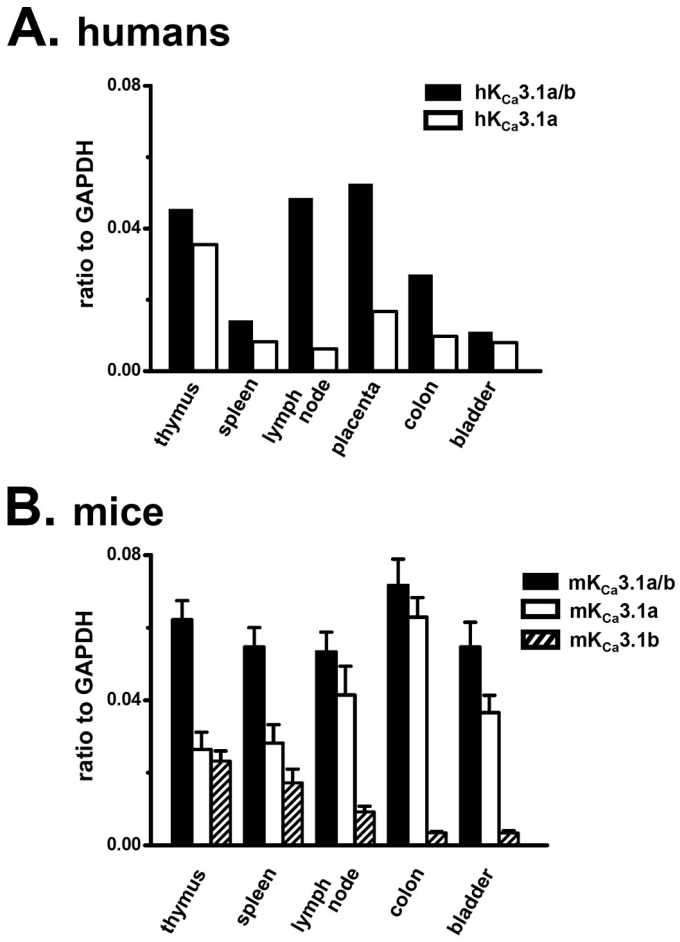

FIGURE 2. **Quantitative real time PCR for $K_{Ca}3.1$ spliced variant expressions in humans (*A*) and mice (*B*) tissues.** Values are shown for steady state transcripts relative to GAPDH in the same preparation. *A*, results are expressed as the means of triplicate analyses. *B*, results are expressed as the means ± S.E. ($n = 5$).

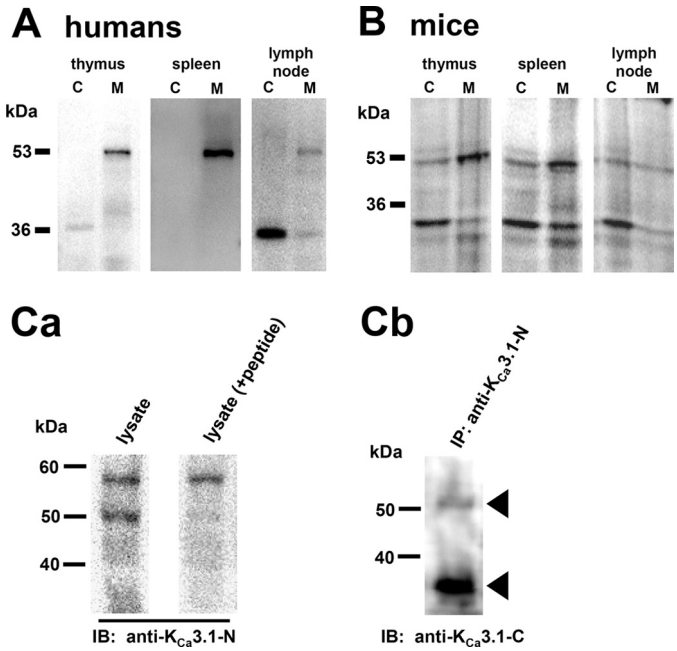

FIGURE 3. $K_{Ca}3.1$ protein expressions in thymus, spleen, and lymph node (mesenteric) of humans (*A*) and mice (*B*). Protein fractions from cytosol (*C*) and plasma membrane (*M*) were probed by immunoblotting with anti-$K_{Ca}3.1$-C antibody. Molecular mass standards are shown in kilodaltons on the *left side* of the panels. *C*, co-immunoprecipitation of $K_{Ca}3.1$b with $K_{Ca}3.1$a. *C, panel a,* plasma membrane protein fraction of mouse thymus was probed by immunoblotting (*IB*) with anti-$K_{Ca}3.1$-C antibody, which recognized the N-terminal region of $K_{Ca}3.1$ (anti-$K_{Ca}3.1$-N) (*left lane*). *Right lane* shows the membrane blotted with $K_{Ca}3.1$-N with excess antigen. *C, panel b,* mouse thymus protein lysate was immunoprecipitated with anti-$K_{Ca}3.1$-N and probed by immunoblotting with anti-$K_{Ca}3.1$-C, which recognized the C terminus of $K_{Ca}3.1$. *Arrowheads* indicate the migrating positions of $K_{Ca}3.1$a (50 kDa) and $K_{Ca}3.1$b (25 kDa). Molecular mass standards are shown in kilodaltons on the *left side* of the panels.

were 0.026 ± 0.005, 0.028 ± 0.005, 0.041 ± 0.008, 0.063 ± 0.005, and 0.037 ± 0.005 in the thymus, spleen, lymph node (mesenteric), colon, and urinary bladder, respectively ($n = 5$ for each), whereas mK$_{Ca}$3.1b expression was 0.023 ± 0.002, 0.017 ± 0.004, 0.009 ± 0.002, 0.003 ± 0.000, and 0.003 ± 0.000 ($n = 5$ for each) (Fig. 2*B*). Similar results were obtained in rat lymphoid tissues (supplemental Fig. S3*A*). Each PCR product was confirmed by DNA sequencing. Taken together, the N terminus lacking the K$_{Ca}$3.1 isoform, K$_{Ca}$3.1b, was also expressed at a significant level in the thymus, spleen, and lymph nodes of rodents.

Protein Expression of $K_{Ca}3.1$ Spliced Variants in Human, Mouse, and Rat Lymphoid Tissues—We calculated the deduced molecular weight of human K$_{Ca}$3.1 spliced variants using GENETYX-Win software version 4.0 (Genetyx Corp., Tokyo, Japan). The deduced molecular masses in hK$_{Ca}$3.1a–d were 36.4, 47.6, 33.2, and 32.7 kDa, respectively. Because anti-K$_{Ca}$3.1 antibody obtained from Alomone Labs was raised against a peptide mapped at the C terminus of K$_{Ca}$3.1, anti-K$_{Ca}$3.1 antibody can recognize not only K$_{Ca}$3.1a but also newly identified K$_{Ca}$3.1 spliced variants. Western blot analyses showed two bands specific for anti-K$_{Ca}$3.1 antibody with molecular masses of 48 and 36 kDa in the plasma membrane and cytosolic fraction of human thymus, spleen, and lymph node (Fig. 3*A*). In particular, a strong 36-kDa band, which was almost identical to the predicted molecular mass of hK$_{Ca}$3.1b, was observed in the cytosolic fraction of human lymph nodes. Similarly, we calculated the deduced molecular mass of mouse and rat K$_{Ca}$3.1 spliced variants, and the calculated molecular masses in mK$_{Ca}$3.1a, mK$_{Ca}$3.1b, rK$_{Ca}$3.1a, and rK$_{Ca}$3.1b were 50.6, 25.0, 47.8, and 30.9 kDa, respectively. In mouse lymphoid tissues (thymus, spleen, and mesenteric lymph node), two bands specific for anti-K$_{Ca}$3.1 antibody with molecular masses of ~50 and 25 kDa were observed in the plasma membrane and cytosolic fractions, respectively (Fig. 3*B*). Similarly, in rat lymphoid tissues, two bands specific for anti-K$_{Ca}$3.1 antibody with molecular masses of ~50 and 30 kDa were observed in the plasma membrane and cytosolic fractions, respectively (supplemental Fig. S3*B*). These signals disappeared by preincubation with the excess antigen, as shown in supplemental Fig. S1 (data not shown), indicating that the N terminus lacking K$_{Ca}$3.1 isoforms was mainly distributed in the cytosolic region but not the plasma membrane in the lymphoid tissues examined. Similar results were obtained from at least three separate experiments.

To determine whether K$_{Ca}$3.1a is immunoprecipitated with these K$_{Ca}$3.1 isoforms, we performed immunoprecipitation using anti-K$_{Ca}$3.1 antibody raised against peptide mapping at the N terminus of K$_{Ca}$3.1, recognizing K$_{Ca}$3.1a but not the N

terminus lacking $K_{Ca}3.1$ isoforms (anti-$K_{Ca}3.1$-N) as a primary antibody for immunoprecipitation. We first confirmed whether anti-$K_{Ca}3.1$-N recognizes $K_{Ca}3.1a$ alone. As shown in Fig. 3*C, panel a,* when anti-$K_{Ca}3.1$-N was used as the primary antibody in Western blot analysis, no band signals with 25 kDa, predicted molecular mass for $mK_{Ca}3.1b$, were observed in membrane fraction proteins from mouse thymus. Signals of 50 kDa, the predicted molecular mass for $mK_{Ca}3.1a$, disappeared by preincubation with excess antigen. We then confirmed the interaction between $mK_{Ca}3.1a$ and $mK_{Ca}3.1b$ using an *in vitro* binding assay with whole tissue lysates of mouse thymus. When immunoprecipitated proteins with anti-$K_{Ca}3.1$-N antibody were stained with anti-$K_{Ca}3.1$-C antibody in Western blotting, a band of 25 kDa for $mK_{Ca}3.1b$ was readily detected (Fig. 3*C, panel b*). These findings suggest that $K_{Ca}3.1a$ strongly interacts with the N terminus lacking $K_{Ca}3.1$ isoforms with a DIS motif in mammalian native tissues.

Cellular Localization of $K_{Ca}3.1$ Spliced Variants in HEK293 Cells—Green fluorescence protein (GFP) relatives, CFP and YFP, have been used extensively to study the subcellular localization of $K_{Ca}3.1$ spliced variants by laser-scanning confocal fluorescence microscopy in living cells. To investigate whether $K_{Ca}3.1$ spliced variants function as trafficking defect isoforms, we examined the cellular localization of $hK_{Ca}3.1$ spliced variants in HEK293 cells, which was transfected with CFP-tagged $hK_{Ca}3.1a$ and/or YFP-tagged $hK_{Ca}3.1b/c/d$. Both fluorescence proteins were tagged to the N termini of $K_{Ca}3.1$ spliced variants. To confirm that the fluorescence protein tag itself does not affect $K_{Ca}3.1a$ channel activity, we performed electrophysiological recordings in transiently CFP-tagged $K_{Ca}3.1a$-expressed HEK293 cells. When whole-cell patch clamp recordings using 500-ms ramps from −120 to 40 mV were performed to assess the level of IK_{Ca} currents under symmetric K^+ conditions, clotrimazole-sensitive IK_{Ca} currents were observed in $hK_{Ca}3.1a$-transfected HEK cells, whereas clotrimazole-sensitive currents were not detectable in mock-transfected HEK293 cells (data not shown). These results are consistent with the functional properties of $hK_{Ca}3.1a$ without CFP tags.

As shown in Fig. 4*A*, in CFP-$hK_{Ca}3.1a$-expressed HEK293 cells, CFP signals were localized along the plasma membrane (Fig. 4*A, panel a*); however, in YFP-$hK_{Ca}3.1b$-expressed HEK293 cells, YFP signals were observed in the whole area of the cells (Fig. 4*A, panel b*). Similar distribution was observed in YFP-$hK_{Ca}3.1c$- and YFP-$hK_{Ca}3.1d$-expressed HEK293 cells, respectively (Fig. 4*A, panels c* and *d*). Of importance, CFP-$hK_{Ca}3.1a$ (*green*) and YFP-$hK_{Ca}3.1b$ signals (*red*) were well overlapped (*yellow*) when CFP-$hK_{Ca}3.1a$ and YFP-$hK_{Ca}3.1b$ were co-expressed in HEK293 cells (Fig. 4*B*). Fig. 4, *C* and *D,* showed the quantitative analyses of CFP/YFP fluorescence intensities, showing that membrane trafficking of $hK_{Ca}3.1a$ was defected by co-expression with $hK_{Ca}3.1b$. Similarly, the co-expression of CFP-$hK_{Ca}3.1a$ with YFP-$hK_{Ca}3.1c$ and YFP-$hK_{Ca}3.1d$ showed the trafficking-defective effects of $hK_{Ca}3.1c$ and $hK_{Ca}3.1d$ in HEK293 cells, respectively (supplemental Fig. S4, *A* and *B*). We also tested the possibility that the co-localization of CFP-$hK_{Ca}3.1a$ with YFP-$hK_{Ca}3.1b/c/d$ was an artifact of bleeding through the emission of light from one fluorophore into the detection range of the other. Cells labeled with only one fluorophore did not result in the detection of light when the filter was set for the other fluorophore (data not shown). $K_{Ca}3.1$ can function as a cell volume regulator (7); however, the diameter of the $K_{Ca}3.1a$-expressed transfectant was not significantly larger than the other spliced isoform-expressed transfectants and native HEK cells (data not shown).

Similar to $hK_{Ca}3.1b$, $mK_{Ca}3.1b$ had a DIS motif, but its molecular weight was smaller than $hK_{Ca}3.1$ (Fig. 1, *A* and *B*); therefore, we examined the trafficking-defective effects of $mK_{Ca}3.1b$ on the cellular localization of $mK_{Ca}3.1a$ in CFP-$mK_{Ca}3.1a$ and YFP-$mK_{Ca}3.1b$-co-expressed HEK293 cells. Similar to the results in human $K_{Ca}3.1$ variants, the trafficking-deficient effects of $mK_{Ca}3.1b$ were clearly observed in CFP-$mK_{Ca}3.1a$ and YFP-$mK_{Ca}3.1b$-co-expressed HEK293 cells, as were the trafficking-deficient effects of $mK_{Ca}3.1a$ by co-expression of $mK_{Ca}3.1b$ (Fig. 5). These results strongly suggest that the N-terminal domain of $K_{Ca}3.1$ may include a critical membrane-trafficking motif and the N terminus lacking $K_{Ca}3.1$ isoforms may function as the dominant negatives of functional $K_{Ca}3.1a$. Additionally, we confirmed no imaging artifacts caused by reciprocal detection of light emitted by CFP or YFP.

Dominant-negative Inhibition of $K_{Ca}3.1a$ Currents by $K_{Ca}3.1$ Spliced Variants—To determine whether $hK_{Ca}3.1b/c/d$ function as dominant-negative isoforms of functional $K_{Ca}3.1a$, electrophysiological experiments were performed using *Xenopus* oocyte expression systems. As shown in Fig. 6*A*, two electrode recordings using a ramp pulse from −120 to 40 mV were performed to assess the level of IK_{Ca} current under physiological conditions, and $hK_{Ca}3.1a$-expressing *X. laevis* oocytes showed ionomycin (0.5 μM) and a potential IK_{Ca} channel opener, DC-EBIO (10 μM)-activated and charybdotoxin (ChTX) (0.1 μM)-inhibited K^+ currents (988.6 ± 112.3 nA at −30 mV, $n = 5$). ChTX-sensitive IK_{Ca} currents were inward at negative potentials, reversed at −80 mV, and showed little rectification. A voltage-gated ChTX-insensitive component was also present, which served as an internal control to demonstrate the specificity of $hK_{Ca}3.1b/c/d$ dominant-inhibitory activity (data not shown). Ionomycin and DC-EBIO had no significant effect on the currents in mock- and water-injected oocytes (data not shown), suggesting that the currents observed in Fig. 6*A* are mostly caused by the expression of $hK_{Ca}3.1a$. When expressed with $hK_{Ca}3.1b/c/d$, they did not produce functional channels ($n = 3$ for each) (see Fig. 6, *B–D*, *right columns*). No ChTX-sensitive currents were observed in water-injected oocytes (data not shown).

We next ascertained whether $hK_{Ca}3.1b/c/d$ exhibited the dominant-inhibitory activity of $hK_{Ca}3.1a$. Co-injection of $hK_{Ca}3.1a$ and $hK_{Ca}3.1b$ cRNAs in the ratios of 1:1 and 1:10 significantly decreased ChTX-sensitive currents at −30 mV in oocytes by 60.7% ($n = 7$) and 10.6% ($n = 3$), respectively ($p <$ 0.05 and 0.01 *versus* $hK_{Ca}3.1a$ alone, $n = 8$) (Fig. 6*B*). Similar to these results, co-injection of $hK_{Ca}3.1a$ and $hK_{Ca}3.1c$ cRNA in the ratios of 1:1 and 1:10 significantly decreased the currents by 15.7% ($n = 7$) and 0.3% ($n = 3$), respectively ($p < 0.01$ *versus* $hK_{Ca}3.1a$ alone, $n = 8$) (Fig. 6*C*), and co-injection of $hK_{Ca}3.1a$ and $hK_{Ca}3.1d$ cRNA in the ratios of 1:1 and 1:10 significantly decreased the currents by 63.8% ($n = 4$) and 12.1% ($n = 3$), respectively ($p < 0.05$ and 0.01 *versus* $hK_{Ca}3.1a$ alone, $n = 5$)

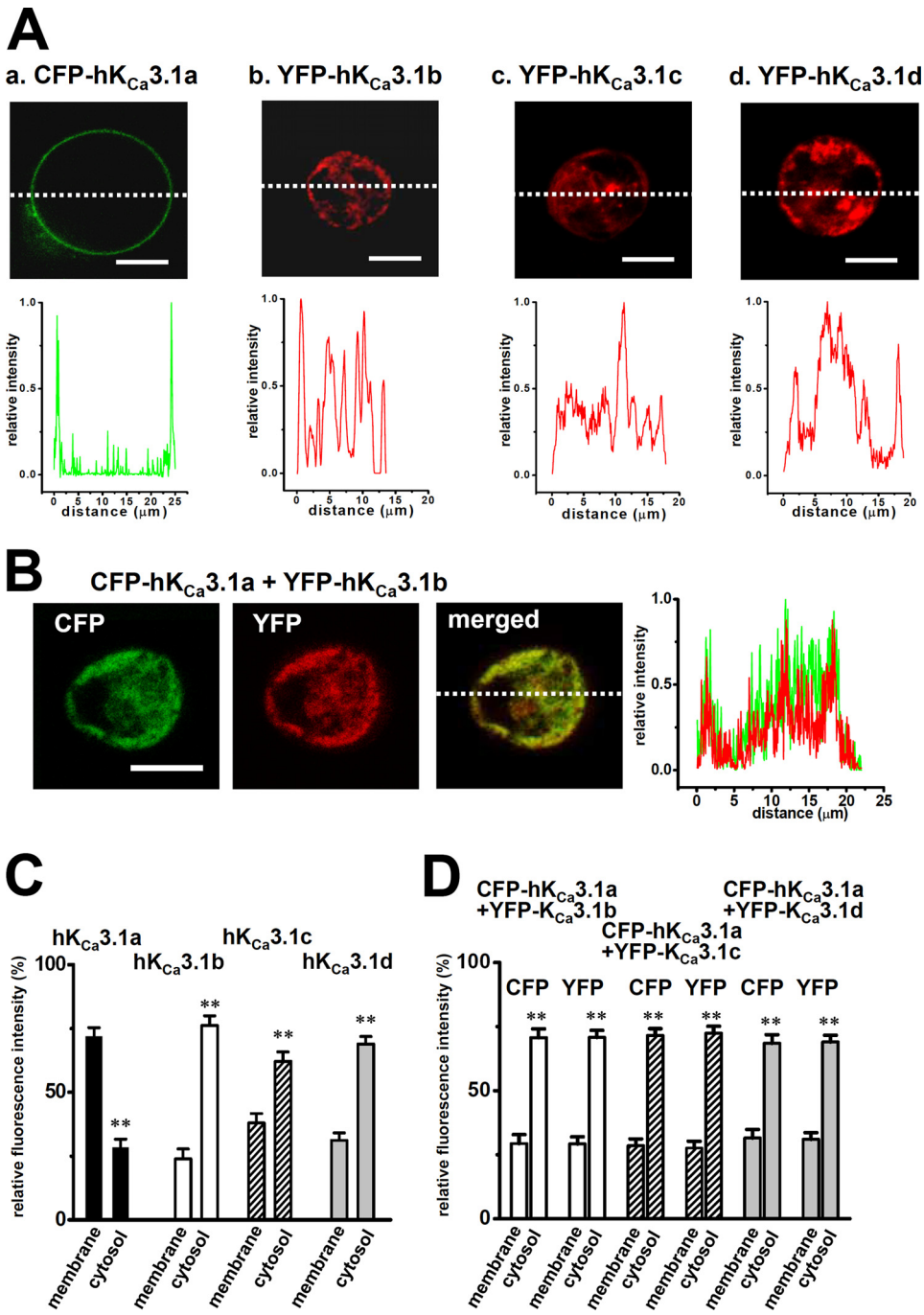

FIGURE 4. **Cellular distribution of human $K_{Ca}3.1$ in HEK293 cells.** *A*, CFP-tagged hK$_{Ca}$3.1a-transfected HEK293 cells, CFP image (*upper panel*) and the profile on the *dotted line* (*lower panel*) are shown in *green* (*panel a*). In YFP-tagged hK$_{Ca}$3.1b/c/d-transfected HEK293 cells, YFP image (*upper panel*) and the profile of relative intensity (*lower panel*) are shown in *red*. *B*, CFP-tagged hK$_{Ca}$3.1a and YFP-tagged hK$_{Ca}$3.1b-cotransfected HEK293 cells, CFP (*upper, left*) and YFP (*upper, right*) images are shown in *green* and *red*, respectively, and the merged image (*lower, left*) and the profiles on the *dotted line* (*lower, right*) of CFP and YFP as *yellow*. *Bar*, 20 μm. *C*, summarized data from *A*. *D*, summarized data from *B* and supplemental Fig. S4. Data are expressed as the means ± S.E. **, $p < 0.01$ *versus* plasma membrane fractions.

(Fig. 6*D*). These clearly indicated that hK$_{Ca}$3.1b/c/d had dominant-negative effects on functional hK$_{Ca}$3.1a channel activity.

Up-regulation of mK$_{Ca}$3.1b in Mouse Thymocytes Isolated without Concanavalin-A Stimulation—To investigate the physiological role of the K$_{Ca}$3.1b spliced isoform in immune cell function, we examined whether the mK$_{Ca}$3.1 isoform expression was altered by the treatment with a T-lymphocyte-selective mitogen, Con-A. Mahaut-Smith and Mason (26) have demonstrated that the earliest events following mitogenic stimulation such as Con-A of thymocytes include an increase in intracellular Ca^{2+} and a concomitant activation of IK$_{Ca}$ channel activity. Mouse thymocytes were isolated in the presence (Con-A(+)) and absence (Con-A(−)) of Con-A, and 60 min later, both cells were cultivated in the presence of Con-A. As shown in Fig. 7*A*, *panel a*, in Con-A(+) thymocytes, the expression levels of both mK$_{Ca}$3.1a and mK$_{Ca}$3.1b transcripts after 0, 1, and 2 day(s) (d0, d1, and d2) were almost similar to those in native thymus tissue (see Fig. 2*B*). Unexpectedly, in Con-A(−)

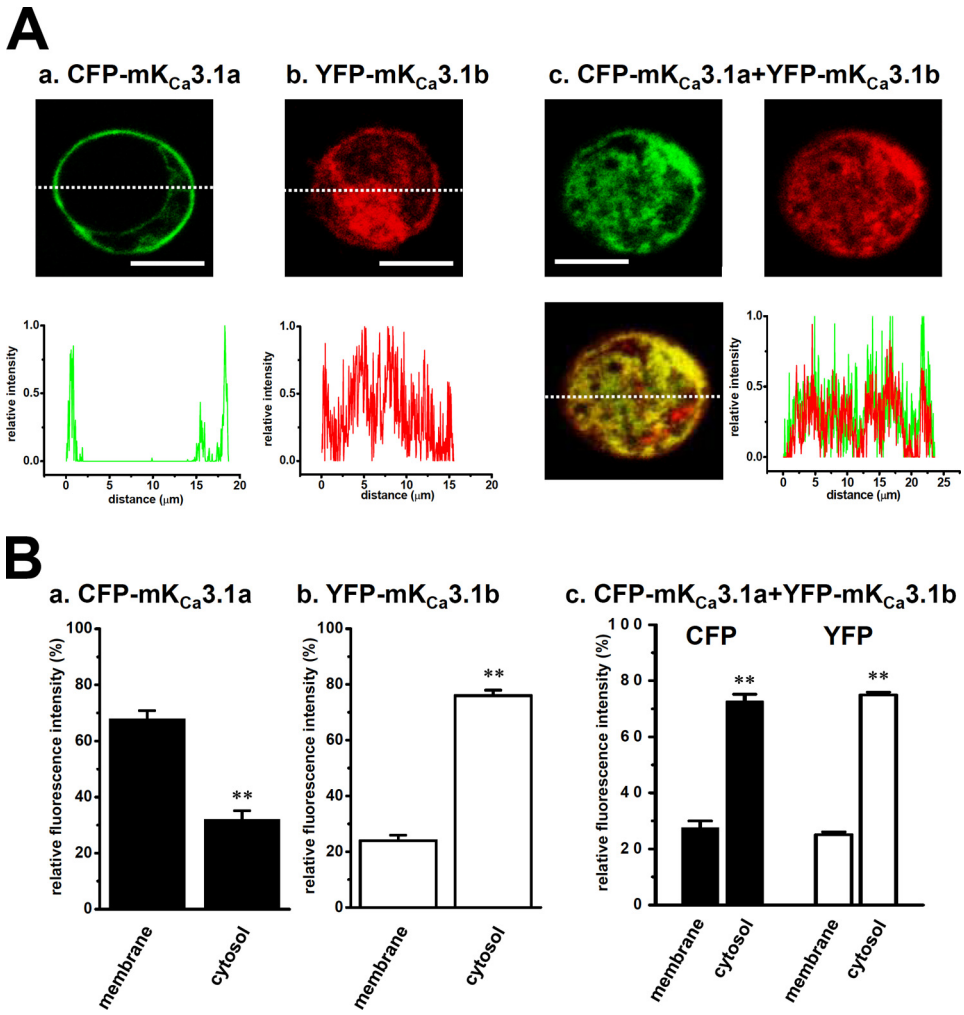

FIGURE 5. **Cellular distribution of murine K_{Ca}3.1 in HEK293 cells.** *A,* CFP-tagged mK$_{Ca}$3.1a-transfected HEK293 cells, CFP image (*upper panel*) and the profile on the *dotted line* (*lower panel*) are shown in *green* (*panel a*). In YFP-tagged mK$_{Ca}$3.1b-transfected HEK293 cells, YFP image (*upper panel*) and the profile on the *dotted line* (*lower panel*) are shown in *red* (*panel b*). In CFP-tagged mK$_{Ca}$3.1a and YFP-tagged mK$_{Ca}$3.1b-co-transfected HEK293 cells, CFP (*upper, left*) and YFP (*upper, right*) images are shown in *green* and *red*, respectively, and the merged image (*lower, left*) and the profiles on the *dotted line* (*lower, right*) of CFP and YFP in *yellow* (*panel c*). *Bar,* 20 μm. *B,* summarized data from *A, panels a–c*. Data are expressed as the means ± S.E. **, $p < 0.01$ *versus* plasma membrane fractions.

thymocytes, the expression of mK$_{Ca}$3.1b transcripts (Fig. 7*A*, *panel b*, *open columns*) was up-regulated with 4–5-fold increase at d1 and d2, without change in mK$_{Ca}$3.1a transcript expression (Fig. 7*A*, *panel b*, *solid columns*) ($n = 5$ for each, $p <$ 0.01 *versus* d0).

Similar to the results of Fig. 3*B*, Western blot assay showed two bands specific for anti-K$_{Ca}$3.1-C antibody with molecular masses of ~50 and 25 kDa in the plasma membrane and cytosolic fraction of thymocytes at d0 (supplemental Fig. S5*A*, *left panel*). Different from thymocytes at d0, mK$_{Ca}$3.1b protein expression in plasma membrane fraction was clearly detected in Con-A(−) thymocytes at d2 (supplemental Fig. S5*A*, *right panel*). Densitometric analyses of anti-K$_{Ca}$3.1-C antibody responses showed significant increase in mK$_{Ca}$3.1b signal in plasma membrane fraction of Con-A(−) thymocytes at d2 ($n =$ 5 for each, $p < 0.01$ *versus* d0) (Fig. 7*B*). Protein expression patterns of mK$_{Ca}$3.1a/b in Con-A(+) thymocytes at d2 were almost identical to those in thymocytes at d0 (data not shown). Positive signals for mK$_{Ca}$3.1a and mK$_{Ca}$3.1b disappeared by preincubation with the excess antigen (data not shown). Additionally, cellular distribution of mK$_{Ca}$3.1 was examined in Con-A(+) and Con-A(−) thymocytes by confocal laser microscope. Similar to Fig. 4*C*, the quantitative analyses of Alexa Fluor 488® fluorescence intensities were performed (Fig. 7*C* and supplemental Fig. S6). When anti-K$_{Ca}$3.1-C antibody was used as a primary antibody, relative fluorescence intensity in the plasma membrane of Con-A(+) thymocytes was significantly higher than in that of Con-A(−) thymocytes (Con-A(+), 62.7 ± 1.7%; Con-A(−), 53.6 ± 1.8%, $n = 16$ for each, $p < 0.01$) (Fig. 7*C*, *solid columns*, and supplemental Fig. S6, *B* and *C*). Moreover, the widths at half-maximum intensity below the plasma membrane of Con-A(+) and Con-A(−) thymocytes were calculated (supplemental Fig. S6, *B* and *C*). The width in Con-A(−) was significantly larger than that in Con-A(+): 0.67 ± 0.09 and 1.21 ± 0.14 mm in Con-A(+) and Con-A(−), respectively ($n = 16$ for each, $p < 0.01$) (Fig. 7*D*). The high level of K$_{Ca}$3.1 expression in plasma membrane were also observed in freshly isolated thymocytes (71.1 ± 2.3%, $n = 10$) (supplemental Fig. S6*A*). We performed similar experiments using anti-K$_{Ca}$3.1-N antibody, recognizing K$_{Ca}$3.1a alone; however, this antibody was not adequate for immunocytochemistry experiments (data not shown). Taken together, mK$_{Ca}$3.1b, which is up-regulated in

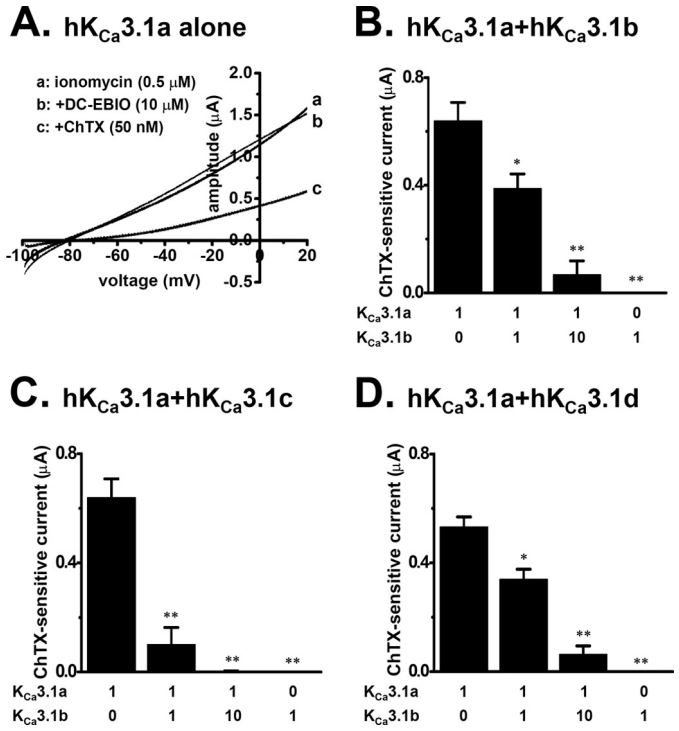

FIGURE 6. **Dominant-negative inhibition of IK_{Ca} currents by $hK_{Ca}3.1$ spliced variants in the *Xenopus* oocyte expression system.** Human $K_{Ca}3.1$ spliced variants were expressed in *Xenopus* oocytes by injection of the corresponding cRNA. *A*, representative traces from oocytes injected with the cRNA for $hK_{Ca}3.1a$. Ionomycin- and DC-EBIO-activated and ChTX-inhibited currents were studied by two-electrode voltage clamp. Current to voltage relations were derived by voltage ramp protocols under physiological conditions. *B–D*, co-expression of $hK_{Ca}3.1b$ (*B*), $hK_{Ca}3.1c$ (*C*), and $hK_{Ca}3.1d$ (*D*) with $hK_{Ca}3.1a$ largely reduced $hK_{Ca}3.1a$-induced IK_{Ca} currents. Current amplitudes were measured at −30 mV. Oocytes were injected with the cRNA for $hK_{Ca}3.1a$ and $hK_{Ca}3.1b/c/d$ at 1:0, 1:1, 1:10, and 0:1 ratios as indicated. Means ± S.E. of current amplitudes from 3 to 8 oocytes for each condition. *, **, $p < 0.05$, 0.01, significantly different as determined by Tukey's test.

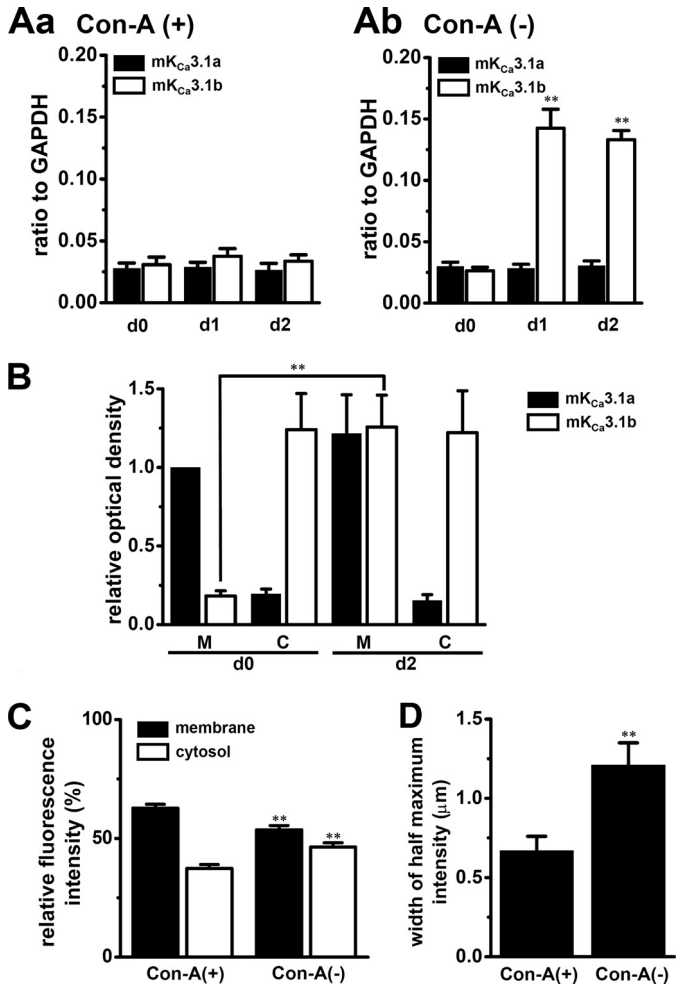

FIGURE 7. **Gene and protein expressions and cellular distribution of $mK_{Ca}3.1$ in Con-A(+) and Con-A(−) thymocytes.** Quantitative real time PCR analysis of $K_{Ca}3.1$ spliced variant expressions in Con-A(+) (*A, panel a*) and Con-A(−) (*A, panel b*) thymocytes at day 0 (*d0*), day 1 (*d1*), and day 2 (*d2*). Values are shown for steady state transcripts relative to GAPDH in the same preparation. Results are expressed as the means ± S.E. ($n = 5$). **, $p < 0.01$ *versus* Con-A(+). *B*, $K_{Ca}3.1$ protein expressions in Con-A(−) thymocytes at d0 and d2. Protein fractions from plasma membrane (*M*) and cytosol (*C*) were probed by immunoblotting with anti-$K_{Ca}3.1$-C antibody. Summarized results were obtained as the optical density of each band signal relative to that of $mK_{Ca}3.1a$ band signal in plasma membrane fraction at d0 ($n = 5$ for each). **, $p < 0.01$ *versus* d0. *C*, summarized data of cellular distribution of $K_{Ca}3.1$ in Con-A(+) and Con-(−) thymocytes. Data are expressed as the means ± S.E. ($n = 16$ for each). **, $p < 0.01$ *versus* Con-A(+). *D*, summarized data of the widths at half-maximum intensity in the plasma membrane of Con-A(+) and Con-A(−) thymocytes. Data are expressed as the means ± S.E. ($n = 16$ for each). **, $p < 0.01$ *versus* Con-A(+).

Con-A(−) thymocytes, may interact with $mK_{Ca}3.1a$ in plasma membrane and suppress functional expression of $mK_{Ca}3.1a$.

Effects of IK_{Ca} Channel Inhibition and Excess $mK_{Ca}3.1b$ Expression on Cell Growth in Mouse Thymocytes—We employed an MTT proliferation assay to determine the effects of up-regulation of $mK_{Ca}3.1b$ on Con-A-stimulated thymocyte growth. Values of living cells were expressed as the ratio of *absorption* spectra of the formed formazan at d2 to that at d0. When isolated thymocytes were cultivated in the absence of Con-A for 2 days, the value of living cells was 0.11 ± 0.01 ($n = 6$) (Fig. 8*A*, *dashed line*). Compared with Con-A(+) thymocytes (Fig. 8*A*, *solid column*, 0.65 ± 0.01, $n = 6$), Con-A(−) thymocytes exhibited significantly reduced levels of living cells at d2 (Fig. 8*A*, *open column*, 0.17 ± 0.01, $n = 6$, $p < 0.01$). Similarly, significant decrease in living cells was observed in Con-A(+) thymocytes by treatment with TRAM-34 in a concentration-dependent manner (1 μM, 0.41 ± 0.01; 10 μM, 0.23 ± 0.03) ($n = 6$ for each, $p < 0.01$ *versus* vehicle (0.1% DMSO, 0.63 ± 0.03)) (Fig. 8*B*). When cultivated in the absence of Con-A for 2 days (including 0.1% DMSO), the value of living cells was 0.14 ± 0.01 ($n = 6$) (Fig. 8*B*, *dashed line*). Several investigations have shown that selective pharmacological $K_{Ca}3.1$ blockade or $K_{Ca}3.1$ deficiency does not promote apoptosis in thymocytes and fibroblasts (5, 27). We quantified apoptotic cells by annexin-V labeling by confocal laser microscopy. In both Con-A(+) and Con-A(−) thymocytes, annexin V-positive cells were less than 1%, and no significant differences were observed. Similarly, application of TRAM-34 produced no increase in annexin V-positive cells. Cell morphology appeared well maintained in all groups examined as visualized by phase contrast microscopy.

We further employed an MTT proliferation assay using $mK_{Ca}3.1b$ overexpressed thymocytes. Under the condition with maximal transfection efficacy, gene and protein expressions of YFP-$mK_{Ca}3.1b$ were determined by real time PCR and Western blot examinations, respectively. As shown in supplemental Fig. S5, *B* and *C*, expressions of both $mK_{Ca}3.1$ transcripts and YFP-$mK_{Ca}3.1b$ (~45 kDa) proteins were signifi-

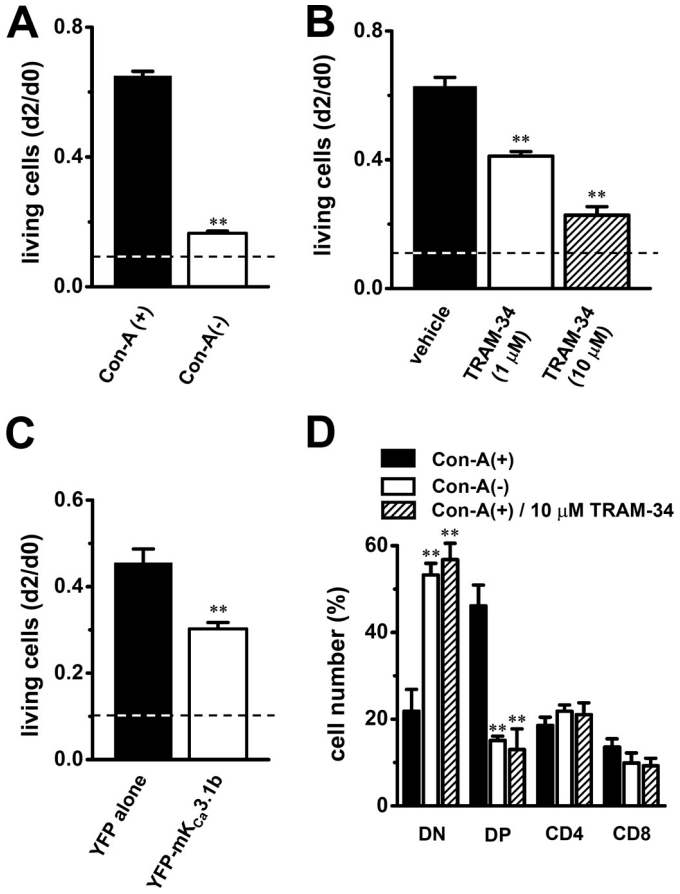

FIGURE 8. **Effects of mK_{Ca}3.1b overexpression and IK_{Ca} current blockade on cell growth and CD4/CD8 phenotype expression in mouse thymocytes.** Cell viability at d2 was evaluated by MTT cell proliferation assay. Value of living cells was expressed as the absorption spectra of the formed formazans and was calculated relative to that in thymocytes at d0. *A,* value of living cells in Con-A(−) thymocytes (*open column*) at d2 was compared with that in Con-A(+) thymocytes (*solid column*) ($n = 6$ for each). **, $p < 0.01$ *versus* Con-A(+). *B,* value of living cells in Con-A(+) thymocytes treated with 1 μM (*open column*) and 10 μM (*hatched column*) TRAM-34 at d2 was compared with that in Con-A(+) thymocytes treated with vehicle (0.1% DMSO) ($n = 6$ for each). **, $p < 0.01$ *versus* vehicle. *C,* value of living cells in Con-A(+) thymocytes transfected with YFP-mK_{Ca}3.1b (*open column*) at d2 was compared with that in Con-A(+) transfected with YFP alone (*solid column*) ($n = 4$ for each). **, $p < 0.01$ *versus* YFP alone. *Dashed lines* show value of living cells in thymocytes cultured in the absence of Con-A. *D,* reduced numbers of CD4(+)CD8(+) double-positive (*DP*) thymocyte populations in Con-A(−) and Con-A(+) treated with TRAM-34. Thymocytes were stained for CD4 and CD8 and examined by flow cytometry. The *bar graph* summarized each subset from separate ($n = 5$ for each) experiments as follows: CD4(−)CD8(−) double-negative (*DN*), CD4(+)CD8(+) double-positive (*DP*), CD4(+)CD8(−) single-positive (*CD4*), and CD4(−)CD8(+) single-positive (*CD8*). **, $p < 0.01$ *versus* Con-A(+).

cantly increased by mK_{Ca}3.1b overexpression. mK_{Ca}3.1-C primer pairs were used for real time PCR (see supplemental Table S1). Only specific band signals in supplemental Fig. S5*C* had disappeared by preincubation of primary antibody with control peptide (data not shown). As shown in Fig. 8*C*, YFP-mK_{Ca}3.1b-expressed Con-A(+) thymocytes (*open column*) exhibited significant reduction of living cells at d2 (YFP alone, 0.45 ± 0.03; YFP-mK_{Ca}3.1b, 0.30 ± 0.01, $n = 4$ for each, $p <$ 0.01). Approximately 15% of YFP-positive cells were observed by flow cytometric analysis. Interestingly, excess expression of human K_{Ca}3.1b, hK_{Ca}3.1b with around 90% (28:31) sequence similarity to mK_{Ca}3.1b in DIS segment, did not produce a significant decrease in living cells (data not shown). Overexpression of mK_{Ca}3.1b produced less than 1% of annexin V-positive cells, and cell morphology appeared well maintained in all groups examined as visualized by phase contrast microscopy.

Flow Cytometric Analysis of Mice Thymocyte Populations—We next examined whether up-regulation of mK_{Ca}3.1b and the inhibition of IK_{Ca} channel activity affected thymocyte phonotypes in Con-A(−) and Con-A(+) treated with TRAM-34 using anti-CD4 and anti-CD8 antibodies by flow cytometry. The percentages of thymocytes showing CD4(−)CD8(−) double-negative (DN), CD4(+)CD8(+) double-positive (DP), CD4(+)CD8(−) single-positive (CD4), and CD4(−)CD8(+) single-positive (CD8) were summarized in Fig. 8*D*. In freshly isolated thymocytes, ~75% of cells showed DP phenotypes (75.7 ± 5.8%, $n = 3$) (supplemental Fig. S7*A*). In Con-A(+) thymocytes, the majority of DP phenotype cells was observed (46.1 ± 4.8%, $n = 5$) (Fig. 8*D*, supplemental Fig. S7*B*); however, in Con-A(−) thymocytes, the differentiation into DN phenotype cells was observed, which represent a minor population in the freshly isolated and Con-A(+) thymocytes (DN: 53.2 ± 2.7%, $n = 5$, $p < 0.01$ *versus* Con-A(+)) (Fig. 8*D* and supplemental Fig. S7*C*). Similarly, the significant decrease in number of DP phenotype cells was observed in Con-A(+) treated with 10 μM TRAM-34 (13.0 ± 4.7%, $n = 4$, $p < 0.01$). No significant differences were observed in CD4 and CD8 phenotype cells between Con-A(+) and Con-A(−) thymocytes (Fig. 8*D*). In thymocytes cultivated in the absence of Con-A for 2 days, over 80% DN phenotype cells were observed (data not shown). These results suggest that up-regulation of mK_{Ca}3.1b may be responsible for the differentiation of DP phenotype cells into DN ones, resulting in the cell growth arrest.

Inhibition of Interleukin-2 Transcription in Thymocytes by Up-regulation of mK_{Ca}3.1b—Interleukin-2 (IL-2) is essential for T cell activation and proliferation. We examined the effects of up-regulation of mK_{Ca}3.1b and inhibition of IK_{Ca} channel activity on the transcription of mice IL-2 (mIL-2) by real time PCR assay. As shown in Fig. 9*A*, ~75% decrease in mIL-2 transcripts was observed in Con-A(−) thymocytes ($n = 4$, $p < 0.01$ *versus* Con-A(+)). Additionally, inhibition of IK_{Ca} channel activity by TRAM-34 (1 and 10 μM) induced the significant decrease in mIL-2 transcription in a concentration-dependent manner (~60 and 70% inhibition, respectively) ($n = 4$ for each, $p < 0.01$ *versus* vehicle) (Fig. 9*B*). In Con-A(+) thymocytes overexpressing YFP-mK_{Ca}3.1b, a significant decrease in mIL-2 transcripts was also observed (~40% inhibition) ($n = 4$, $p <$ 0.01 *versus* YFP alone) (Fig. 9*C*). These suggest that the decrease in mIL-2 transcription may be at least in part involved in the cell growth arrest in thymocytes overexpressing mK_{Ca}3.1b.

DISCUSSION

In this study, we identified the N terminus lacking spliced variants of the intermediate conductance Ca^{2+}-activated K^+ channel, K_{Ca}3.1 (K_{Ca}3.1-ΔN), from lymphoid tissues of human and rodents. K_{Ca}3.1-ΔN isoforms have dominant-negative effects on membrane trafficking and the channel activity of functional K_{Ca}3.1a, suggesting that, in addition to the up-regulation of K_{Ca}3.1a, down-regulation of K_{Ca}3.1-ΔN may also be associated with the mechanisms underlying the enhancement

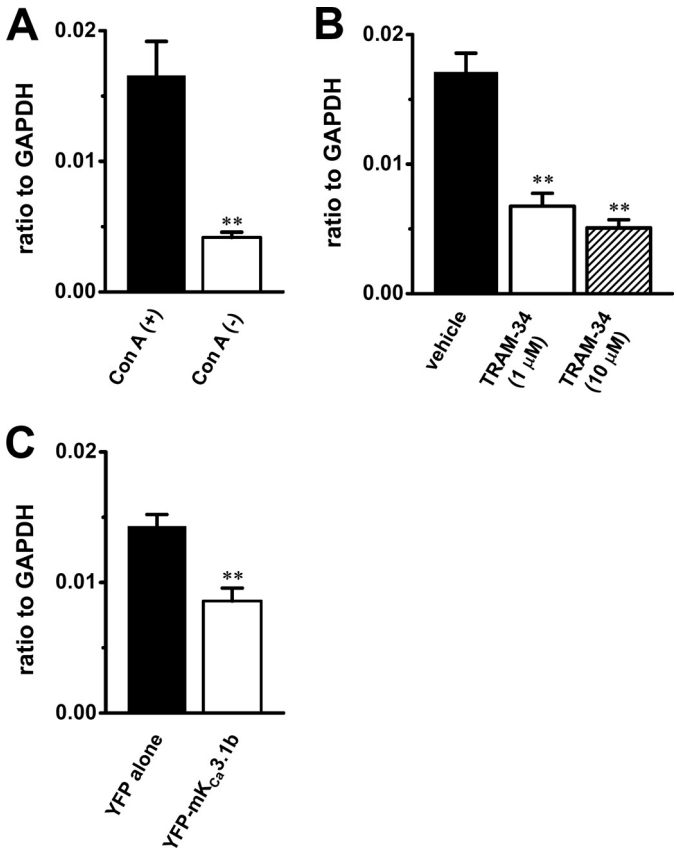

FIGURE 9. **Quantitative real time PCR for interleukin-2 expression in mouse thymocytes.** *A, closed* and *open columns* show interleukin-2 expression in Con-A(+) and Con-A(−) thymocytes, respectively. Values are shown for steady state transcripts relative to GAPDH in the same preparation ($n = 4$ for each, $p < 0.01$). *B, closed, open,* and *hatched columns* show interleukin-2 expression in Con-A(+) thymocytes treated with vehicle (0.1% DMSO), 1 μM TRAM-34, and 10 μM TRAM-34, respectively ($n = 4$ for each, $p < 0.01$ *versus* vehicle). *C, closed* and *open columns* show interleukin-2 expression in Con-A(+) thymocytes transfected with pEYFP-C (YFP alone) and pEYFP-mK$_{Ca}$3.1b (YFP-mK$_{Ca}$3.1b), respectively ($n = 4$ for each, $p < 0.01$).

of IK$_{Ca}$ channel activity in activated T-lymphocytes. Additionally, we indicated that up-regulation of mK$_{Ca}$3.1b in mouse thymocytes differentiated CD4(+)CD8(+) DP phenotype thymocytes into CD4(−)CD8(−) DN ones, which represent a minor population in the native thymus, and suppressed Con-A-stimulated thymocyte growth by down-regulation of mIL-2 transcripts. The role of K$_{Ca}$3.1b in mouse thymocytes was also confirmed by generating mK$_{Ca}$3.1b-overexpressing thymocytes.

N Terminus of K_{Ca} Critical for Channel Trafficking to Plasma Membrane—In voltage-gated K^+ (K_v) channels, it is well known that the cytoplasmic N- and C-terminal domains modify channel gating, membrane trafficking, and protein degradation (28–30). Several investigations have shown that the N-terminal domains of K$_{Ca}$3.1 and K$_{Ca}$2.*x* with a similar intron-exon structure to K$_{Ca}$3.1 play an important role for channel assembly and membrane trafficking using the N terminus lacking recombinant mutants and N-terminal polypeptides (6, 14, 19, 20, 31–33); however, K$_{Ca}$3.1 alternative splicing has not been identified in native tissues. This is the first identification of K$_{Ca}$3.1-ΔN variants significantly expressed in human and rodent lymphoid organs (Figs. 1–3, andsupplemental Fig. S3). Alternative splicing patterns differed among species in various tissues (supplemental Fig. S2); however, the most dominant was commonly K$_{Ca}$3.1b in human and rodent lymphoid tissues. K$_{Ca}$3.1-ΔN exerted the membrane-trafficking inhibition of K$_{Ca}$3.1a proteins (Figs. 4 and 5 and supplemental Fig. S4) and the dominant-negative effects of its activity (Fig. 6) by the formation of interaction partners with K$_{Ca}$3.1a (Fig. 3*C*). This inhibitory effect of alternative splicing on IK$_{Ca}$ channel activity may be involved in the abnormalities in T cell function and its related diseases by K$_{Ca}$3.1 dysfunction. Indeed, disruption of K$_{Ca}$3.1 channel function by up-regulation of mK$_{Ca}$3.1b and pharmacological blockade of IK$_{Ca}$ channel activity was associated with the cell growth arrest and the cell differentiation into CD4/CD8 subsets in mouse thymocytes (Fig. 8).

Different from the cellular distribution of mK$_{Ca}$3.1b proteins in mK$_{Ca}$3.1a/b-co-expressed HEK293 cells (Fig. 5, *A, panel c,* and *B, panel c*), mK$_{Ca}$3.1b proteins in Con-A(−) thymocytes distributed to plasma membrane fraction at a relatively abundant level (Fig. 7, *B* and *C,* and supplemental Fig. S5*A*). We identified the interacting proteins with the C-terminal domain of K$_{Ca}$3.1 using the yeast two-hybrid system, and we isolated a cytoskeletal protein, spectrin α, nonerythrocytic 1 (SPTAN1) and a targeting protein to plasma membrane, FYN tyrosine kinase.[3] In lymphocytes, spectrin is aggregated to a discrete region of plasma membrane (34). Therefore, this discrepancy of K$_{Ca}$3.1b distribution can be explained by the interaction of the C terminus of K$_{Ca}$3.1b with cytoskeletal and membrane-targeting proteins in native thymocytes. Indeed, K$_{Ca}$3.1 proteins in Con-A(−) thymocytes distributed in a wider area below the plasma membrane, in comparison with those in Con-A(+) thymocytes (Fig. 7*D*).

Possible Pathophysiological Significances of $K_{Ca}3.1$ Alternative Splicing—Alternative splicing can result in significant changes in the original function in various disease pathogeneses; for example, the N-terminal truncated isoform of K$_{Ca}$2.3, K$_{Ca}$2.3–1B, is implicated in schizophrenia as a potent dominant-negative regulator of K$_{Ca}$2.3 (18). In a chronic inflammatory disease, multiple sclerosis and experimental autoimmune encephalomyelitis animal model with similarities to multiple sclerosis in pathogenicity, alternative splicing of several genes has been reported (35–37). Functional regulation of immune response-related molecules by alternative splicing during cell proliferation and differentiation is therefore expected to provide new therapeutic strategies for the treatment of immune diseases (38). K$_{Ca}$3.1 is involved in the proliferation and differentiation of naive and central memory T-lymphocytes (39–41), and also relatively higher levels of IK$_{Ca}$ channel activity are detected in Th1 cells compared with Th2 cells (42). Cell type-specific and disease-associated alternative splicing of K$_{Ca}$3.1 has not been found yet; however, the increase in IK$_{Ca}$ channel activity by the down-regulation of K$_{Ca}$3.1-ΔN may have potential in the pathogenesis of Th1-mediated autoimmune diseases, such as multiple sclerosis and delayed-type hypersensitivity.

In addition, K$_{Ca}$3.1 gene expression is positively regulated by activator protein-1 (AP-1, Fos/Jun complex) and Ikaros-2 and negatively regulated by repressor element 1-silencing tran-

[3] S. Ohya, unpublished data.

scription factor (REST) (40, 43). Recent studies have reported that N-terminal spliced variants of Ca^{2+}- and Na^{+}-activated K^{+} channels (Slo/$K_{Ca}1.1$ and Slack/$K_{Ca}4.1$) are regulated by alternative promoters (44, 45). As shown in Figs. 2 and 3, the expression pattern of $K_{Ca}3.1a$ and $K_{Ca}3.1b$ was quite different between the thymus and mesenteric lymph node, suggesting that the alternative transcriptional regulators of $K_{Ca}3.1$ described above may be responsible for the tissue-specific and cell type-specific expressions of $K_{Ca}3.1$ alternative transcripts. A recent study has shown that alternative splicing of $K_{Ca}1.1$ is post-transcriptionally regulated by microRNA (46). Future investigations will provide new insight into post-transcriptional regulation of $K_{Ca}3.1$ splicing by microRNA.

Membrane depolarization induced by IK_{Ca} channel blockade suppresses Ca^{2+} influx through a Ca^{2+} release-activated Ca^{2+} channel in T-lymphocytes (47, 48). Membrane depolarization also causes up-regulation of cyclin-dependent kinase inhibitor $p27^{Kip1}$ and a subsequent cell cycle arrest in phase G_0/G_1 in several types of cells, including T-lymphocytes (49–51). These are strongly associated with the suppression of IL-2 transcription/production, and thereby T cell proliferation and differentiation are inhibited (50–53). In this study, we indicated that up-regulation of $mK_{Ca}3.1b$ and pharmacological blockade of IK_{Ca} channel activity suppressed cell growth, IL-2 transcription, and maintenance of CD4(+)CD8(+) DP phenotype in mouse thymocytes (Figs. 8 and 9). In Con-A(−) and TRAM-34-treated Con-A(+) thymocytes, expression of $p27^{Kip1}$ transcripts was ~2-fold up-regulated, compared with that in Con-A(+) thymocytes (supplemental Fig. S8). These results suggest that $K_{Ca}3.1b$ may be responsible for the fine-tuning of such signaling pathways in T-lymphocytes and may play a key regulatory role in governing the termination of immune response in T-lymphocytes.

A balance between the translation and degradation of ion channels is also of importance to regulate its activity. It has been reported that the N termini of $K_{Ca}2.3$ and $K_{Ca}3.1$ play an important role in shuttling them to the proteasome for degradation with a different mechanism (54, 55). Gao *et al.* (54) have clarified that S3/S4 domains are essential for the degradation of $K_{Ca}3.1$ proteins. As shown in Fig. 1, $K_{Ca}3.1b$ isolated from human and rodent thymus lacked S3 and/or S4 domains; therefore, the lack of these domains in $K_{Ca}3.1b$ could relate to a discrepancy between the results of real time PCR and Western blotting examinations, particularly observed in mouse lymph nodes (Figs. 2*B* and 3*B*). In addition to the post-transcriptional regulation of $K_{Ca}3.1$, the differences in protein degradation between $K_{Ca}3.1a$ and $K_{Ca}3.1b$ may be an important mechanism underlying the physiological and pathophysiological regulation of IK_{Ca} channel activity.

In conclusion, this is the first time that novel alternative splicing of the $K_{Ca}3.1$ gene in the N terminus has been identified in the lymphoid tissues of humans and rodents with their evident trafficking-defective and functionally dominant-negative effects on the original $K_{Ca}3.1a$. The putative molecular mechanism underlying the generation of alternative splicing of $K_{Ca}3.1$ remains to be determined; however, the novel regulation of the alternative splicing of $K_{Ca}3.1$ may play important roles in physiological and pathophysiological settings. This study strongly suggests that the altered combinatorial splicing profiles of $K_{Ca}3.1$ transcripts may provide a different and new perspective in understanding their role in generating autoimmune disorders, cancer, and restenosis, and the dominant negatives may be new targets and markers for diseases generated by $K_{Ca}3.1$ dysfunction.

Acknowledgment—We thank Dr. Shimada (Osaka University, Japan) for the gift of the plasmid vector for Xenopus oocyte expression.

REFERENCES

1. Ghatta, S., Nimmagadda, D., Xu, X., and O'Rourke, S. T. (2006) *Pharmacol. Ther.* **110,** 103–116
2. Stocker, M. (2004) *Nat. Rev. Neurosci.* **5,** 758–770
3. Logsdon, N. J., Kang, J., Togo, J. A., Christian, E. P., and Aiyar, J. (1997) *J. Biol. Chem.* **272,** 32723–32726
4. Köhler, M., Hirschberg, B., Bond, C. T., Kinzie, J. M., Marrion, N. V., Maylie, J., and Adelman, J. P. (1996) *Science* **273,** 1709–1714
5. Begenisich, T., Nakamoto, T., Ovitt, C. E., Nehrke, K., Brugnara, C., Alper, S. L., and Melvin, J. E. (2004) *J. Biol. Chem.* **279,** 47681–47687
6. Fanger, C. M., Rauer, H., Neben, A. L., Miller, M. J., Rauer, H., Wulff, H., Rosa, J. C., Ganellin, C. R., Chandy, K. G., and Cahalan, M. D. (2001) *J. Biol. Chem.* **276,** 12249–12256
7. Elliott, J. I., and Higgins, C. F. (2003) *EMBO Rep.* **4,** 189–194
8. Jensen, B. S., Strøbaek, D., Olesen, S. P., and Christophersen, P. (2001) *Curr. Drug Targets* **2,** 401–422
9. Köhler, R., Wulff, H., Eichler, I., Kneifel, M., Neumann, D., Knorr, A., Grgic, I., Kämpfe, D., Si, H., Wibawa, J., Real, R., Borner, K., Brakemeier, S., Orzechowski, H. D., Reusch, H. P., Paul, M., Chandy, K. G., and Hoyer, J. (2003) *Circulation* **108,** 1119–1125
10. Chandy, K. G., Wulff, H., Beeton, C., Pennington, M., Gutman, G. A., and Cahalan, M. D. (2004) *Trends Pharmacol. Sci.* **25,** 280–289
11. Wulff, H., and Pennington, M. (2007) *Curr. Opin. Drug Discov. Devel.* **10,** 438–445
12. Ishii, T. M., Silvia, C., Hirschberg, B., Bond, C. T., Adelman, J. P., and Maylie, J. (1997) *Proc. Natl. Acad. Sci. U.S.A.* **94,** 11651–11656
13. Joiner, W. J., Wang, L. Y., Tang, M. D., and Kaczmarek, L. K. (1997) *Proc. Natl. Acad. Sci. U.S.A.* **94,** 11013–11018
14. Miller, M. J., Rauer, H., Tomita, H., Rauer, H., Gargus, J. J., Gutman, G. A., Cahalan, M. D., and Chandy, K. G. (2001) *J. Biol. Chem.* **276,** 27753–27756
15. Monaghan, A. S., Benton, D. C., Bahia, P. K., Hosseini, R., Shah, Y. A., Haylett, D. G., and Moss, G. W. (2004) *J. Biol. Chem.* **279,** 1003–1009
16. Snyders, D. J. (1999) *Cardiovasc. Res.* **42,** 377–390
17. Kolski-Andreaco, A., Tomita, H., Shakkottai, V. G., Gutman, G. A., Cahalan, M. D., Gargus, J. J., and Chandy, K. G. (2004) *J. Biol. Chem.* **279,** 6893–6904
18. Tomita, H., Shakkottai, V. G., Gutman, G. A., Sun, G., Bunney, W. E., Cahalan, M. D., Chandy, K. G., and Gargus, J. J. (2003) *Mol. Psychiatry* **8,** 524–535
19. Joiner, W. J., Khanna, R., Schlichter, L. C., and Kaczmarek, L. K. (2001) *J. Biol. Chem.* **276,** 37980–37985
20. Syme, C. A., Hamilton, K. L., Jones, H. M., Gerlach, A. C., Giltinan, L., Papworth, G. D., Watkins, S. C., Bradbury, N. A., and Devor, D. C. (2003) *J. Biol. Chem.* **278,** 8476–8486
21. Ohya, S., Kuwata, Y., Sakamoto, K., Muraki, K., and Imaizumi, Y. (2005) *Am. J. Physiol. Heart Circ. Physiol.* **289,** H1635–H1642
22. Ohya, S., Takii, T., Yamazaki, H. F., Matsumori, M., Onozaki, K., Watanabe, M., and Imaizumi, Y. (1997) *FEBS Lett.* **401,** 252–258
23. Deleted in proof
24. Deleted in proof
25. Ghanshani, S., Coleman, M., Gustavsson, P., Wu, A. C., Gargus, J. J., Gutman, G. A., Dahl, N., Mohrenweiser, H., and Chandy, K. G. (1998) *Genomics* **51,** 160–161
26. Mahaut-Smith, M. P., and Mason, M. J. (1991) *J. Physiol.* **439,** 513–528
27. Grgic, I., Kiss, E., Kaistha, B. P., Busch, C., Kloss, M., Sautter, J., Müller, A.,

Kaistha, A., Schmidt, C., Raman, G., Wulff, H., Strutz, F., Gröne, H. J., Köhler, R., and Hoyer, J. (2009) *Proc. Natl. Acad. Sci. U.S.A.* **106,** 14518–14523
28. Hopkins, W. F., Demas, V., and Tempel, B. L. (1994) *J. Neurosci.* **14,** 1385–1393
29. Levitan, E. S., and Takimoto, K. (2000) *Trends Cardiovasc. Med.* **10,** 317–320
30. Strang, C., Cushman, S. J., DeRubeis, D., Peterson, D., and Pfaffinger, P. J. (2001) *J. Biol. Chem.* **276,** 28493–28502
31. Roncarati, R., Decimo, I., and Fumagalli, G. (2005) *Mol. Cell. Neurosci.* **28,** 314–325
32. Decimo, I., Roncarati, R., Grasso, S., Clemens, M., Chiamulera, C., and Fumagalli, G. (2006) *Biosci. Rep.* **26,** 399–412
33. Srivastava, S., Choudhury, P., Li, Z., Liu, G., Nadkarni, V., Ko, K., Coetzee, W. A., and Skolnik, E. Y. (2006) *Mol. Biol. Cell* **17,** 146–154
34. Pauly, J. L., Bankert, R. B., and Repasky, E. A. (1986) *J. Immunol.* **136,** 246–253
35. Lundmark, F., Duvefelt, K., Iacobaeus, E., Kockum, I., Wallström, E., Khademi, M., Oturai, A., Ryder, L. P., Saarela, J., Harbo, H. F., Celius, E. G., Salter, H., Olsson, T., and Hillert, J. (2007) *Nat. Genet.* **39,** 1108–1113
36. Gillett, A., Maratou, K., Fewings, C., Harris, R. A., Jagodic, M., Aitman, T., and Olsson, T. (2009) *PLoS ONE* **4,** e7773
37. Hu, X., Barnum, S. R., Wohler, J. E., Schoeb, T. R., and Bullard, D. C. (2010) *Mol. Immunol.* **47,** 1692–1700
38. Mourich, D. V., and Iversen, P. L. (2009) *Curr. Opin. Mol. Ther.* **11,** 124–132
39. Wulff, H., Beeton, C., and Chandy, K. G. (2003) *Curr. Opin. Drug Discov. Devel.* **6,** 640–647
40. Ghanshani, S., Wulff, H., Miller, M. J., Rohm, H., Neben, A., Gutman, G. A., Cahalan, M. D., and Chandy, K. G. (2000) *J. Biol. Chem.* **275,** 37137–37149
41. Cahalan, M. D., and Chandy, K. G. (2009) *Immunol. Rev.* **231,** 59–87
42. Fanger, C. M., Neben, A. L., and Cahalan, M. D. (2000) *J. Immunol.* **164,** 1153–1160
43. Cheong, A., Bingham, A. J., Li, J., Kumar, B., Sukumar, P., Munsch, C., Buckley, N. J., Neylon, C. B., Porter, K. E., Beech, D. J., and Wood, I. C. (2005) *Mol. Cell* **20,** 45–52
44. Brenner, R., Thomas, T. O., Becker, M. N., and Atkinson, N. S. (1996) *J. Neurosci.* **16,** 1827–1835
45. Brown, M. R., Kronengold, J., Gazula, V. R., Spilianakis, C. G., Flavell, R. A., von Hehn, C. A., Bhattacharjee, A., and Kaczmarek, L. K. (2008) *J. Physiol.* **586,** 5161–5179
46. Pietrzykowski, A. Z., Friesen, R. M., Martin, G. E., Puig, S. I., Nowak, C. L., Wynne, P. M., Siegelmann, H. T., and Treistman, S. N. (2008) *Neuron* **59,** 274–287
47. Deleted in proof
48. Hogan, P. G., Lewis, R. S., and Rao, A. (2010) *Annu. Rev. Immunol.* **38,** 491–533
49. Boussiotis, V. A., Freeman, G. J., Taylor, P. A., Berezovskaya, A., Grass, I., Blazar, B. R., and Nadler, L. M. (2000) *Nat. Med.* **6,** 290–297
50. Ghiani, C. A., Yuan, X., Eisen, A. M., Knutson, P. L., DePinho, R. A., McBain, C. J., and Gallo, V. (1999) *J. Neurosci.* **19,** 5380–5392
51. Dohda, T., Maljukova, A., Liu, L., Heyman, M., Grandér, D., Brodin, D., Sangfelt, O., and Lendahl, U. (2007) *Exp. Cell Res.* **313,** 3141–3152
52. Wonderlin, W. F., and Strobl, J. S. (1996) *J. Membr. Biol.* **154,** 91–107
53. Di, L., Srivastava, S., Zhdanova, O., Ding, Y., Li, Z., Wulff, H., Lafaille, M., and Skolnik, E. Y. (2010) *Proc. Natl. Acad. Sci. U.S.A.* **107,** 1541–1546
54. Gao, Y., Chotoo, C. K., Balut, C. M., Sun, F., Bailey, M. A., and Devor, D. C. (2008) *J. Biol. Chem.* **283,** 9049–9059
55. Gao, Y., Balut, C. M., Bailey, M. A., Patino-Lopez, G., Shaw, S., and Devor, D. C. (2010) *J. Biol. Chem.* **285,** 17938–17953